RAA 2016 Vol. **16** No. **9**, 140 (10pp) doi: 10.1088/1674–4527/16/9/140
http://www.raa-journal.org *http://iopscience.iop.org/raa*

***R**esearch in*
***A**stronomy and*
***A**strophysics*

Estimating stellar effective temperatures and detected angular parameters using stochastic particle swarm optimization

Chuan-Xin Zhang, Yuan Yuan, Hao-Wei Zhang, Yong Shuai and He-Ping Tan

School of Energy Science and Engineering, Harbin Institute of Technology, Harbin 150001, China;
yuanyuan83@hit.edu.cn

Received 2016 February 20; accepted 2016 April 28

Abstract Considering features of stellar spectral radiation and sky surveys, we established a computational model for stellar effective temperatures, detected angular parameters and gray rates. Using known stellar flux data in some bands, we estimated stellar effective temperatures and detected angular parameters using stochastic particle swarm optimization (SPSO). We first verified the reliability of SPSO, and then determined reasonable parameters that produced highly accurate estimates under certain gray deviation levels. Finally, we calculated 177 860 stellar effective temperatures and detected angular parameters using data from the Midcourse Space Experiment (MSX) catalog. These derived stellar effective temperatures were accurate when we compared them to known values from literatures. This research makes full use of catalog data and presents an original technique for studying stellar characteristics. It proposes a novel method for calculating stellar effective temperatures and detecting angular parameters, and provides theoretical and practical data for finding information about radiation in any band.

Key words: physical data and process: radiative transfer — methods: data analysis — astronomical databases: miscellaneous — stars: atmospheres

1 INTRODUCTION

In order to obviously (Ahn et al. 2012) distinguish targets in sky surveys, appropriate detection bands need to be selected. The bands used by existing large scale sky surveys are listed in Table 1 (Neugebauer et al. 1984; Wright et al. 2010; Skrutskie et al. 2006; Ishihara et al. 2010; Egan et al. 2003; Ahn et al. 2012; Zhao et al. 2012; Kordopatis et al. 2013; Steinmetz et al. 2006; Aihara et al. 2011; Xiang et al. 2015; Yuan et al. 2015; Luo et al. 2015). The detected bands that already exist are not comprehensive, and the flux density across large ranges of wavelength cannot be obtained. In other words, stellar radiation energy cannot be obtained in some other bands, but we need information about energy in those bands. It is therefore important to develop methods to determine the required information about radiation from existing data. It is important to derive stellar atmospheric parameters (including stellar effective temperatures, surface gravity and chemical abundances) from different stellar spectral data. Stellar effective temperatures effect luminosities and spectral characteristics, and they are also closely related to stellar physical properties, chemical compositions and stellar evolution (Huang et al. 2015). Thus, if we can obtain stellar effective temperatures and detected angular parameters, we can reduce the complexity of this problem and derive the radiation energy of any band.

A star's color is determined by its effective temperature. Preliminary information about stars such as effective temperatures can be obtained from the stellar color or approximate spectral type. We can calculate stellar physical parameters from low-resolution spectra using the Indirect Calculation Method, Infrared Flux Method, Template Matching Method, Neural Network Method, Non-parametric Estimation Method, Color Selection Method, and so forth. The Indirect Calculation Method is used to find the effective temperatures of a star using the distance between the star and the Earth, and the brightness of the star. Blackwell & Shallis (1977) and Blackwell et al. (1980) used the Infrared Flux Method to calculate stellar effective temperatures and angular diameters. This approach needs a precise sequence of infrared and temperature data. However, precise data regarding these physical properties can only be determined for a limited number of stars, regardless of what method they use. Only a small number of stars have been precisely measured. Soubiran et al. (1998) and Katz et al. (1998) established a stellar spectral template library including 211 stars. They used the Nearest Neighbor Method to calculate stellar spectral radiation fluxes. Bailer-Jones (2000) calculated synthetic spectra and stellar spectral radiation fluxes using the Neural Network Method. Zhang et al. (2005) proposed fitting and estimating stellar effective temperatures using a polynomial exponential model and the Non-parametric

Table 1 Sky Survey and Detection Bands

Probe name	Detection bands (μm)
Infrared Astronomical Satellite (IRAS)	12, 25, 60, 100
Wide-field Infrared Survey Explorer (WISE)	3.4, 4.6, 12, 22
Two Micron All Sky Survey (2MASS)	1.25, 1.65, 2.17
AKARI , previously called InfraRed Imaging Surveyor (IRIS)	9, 18
Midcourse Space Experiment (MSX)	4.25, 4.29, 8.23, 12.13, 14.65, 21.34
Sloan Digital Sky Survey (SDSS)	0.3551, 0.4686, 0.6166, 0.748, 0.8932
Large sky Area Multi-Object Fiber Spectroscopic Telescope (LAMOST)	0.37–0.9

Estimation Method. They first decomposed spectral data using Principal Component Analysis (PCA). They then derived the fitting surface of the polynomial exponential function that corresponded to its surface temperature using the PCA data. Stellar surface temperatures were calculated using the final resulting polynomial logarithmic function. Engelke et al. (2006) composed a library of stellar spectral templates using spectral data fragments that were recorded by spectrometers. They used the spectral template technique proposed by Cohen (1993), in which any segment of spectral radiation flux can be fitted and composed using this spectral template library. However, it is not accurate and fundamental stellar information (including stellar effective temperatures and detection angles) was not calculated. Rebassa-Mansergas et al. (2010, 2012, 2013) searched for white dwarf-main sequence binaries using template matching and the Color Selection Method based on optical and infrared photometry from the Sloan Digital Sky Survey (SDSS). Ren et al. (2014) calculated stellar temperatures using the Template Matching Method, and estimated the distance of DA/M binaries. They focused on white dwarf-main sequence binaries.

The above summary shows that existing publications mainly used star catalog data and spectral template technology to calculate stellar atmospheric parameters. Most models used star catalogs to directly record stellar radiation energy, and simulated bands are limited. Based on this, we applied a particle swarm optimization algorithm to these data to calculate effective stellar temperatures and detected angular parameters considering stellar radiation flux data from surveys. These two parameters can be used to indirectly calculate radiation energy of any band that is required. In this work, we investigated impacts of algorithmic parameters, gray deviations and the selection of observed samples on inversion results. We also analyzed the performance of inversion models and determined the optimal inversion parameters. We compared our results with known data to verify the accuracy and applicability of the inversion model.

2 METHODS

2.1 Stellar Effective Temperature Model

Stars have characteristics that are similar to blackbodies. However, the presence of gases at different temperatures, pressures and densities on the stellar surface means that some bands have significant absorption or emission lines. It is important that we study gases and characteristics of stellar surfaces in relation to these absorption or emission lines. If the stellar atmosphere is supposed to be in a state of thermodynamic equilibrium, stellar surface temperatures can be calculated using the relevant blackbody radiation formula. Assuming stars have similar spectral emissivity and gray characteristics (as discussed later in this article), if these parameters can meet our requirements regarding detection accuracy, then this assumption is valid. Planck's law describes the electromagnetic radiation emitted by a blackbody in thermal equilibrium at a definite temperature, and that the spectral emissive power of the blackbody in some bands is

$$E_{\mathrm{b}(\lambda_1-\lambda_2)} = \int_{\lambda_1}^{\lambda_2} \frac{c_1\lambda^{-5}}{\exp[c_2/(\lambda T)]-1} d\lambda. \quad (1)$$

Here, $E_{\mathrm{b}(\lambda_1-\lambda_2)}$ represents the spectral emissive power of the blackbody from λ_1 to λ_2 ($\mathrm{W}\cdot\mathrm{m}^{-2}$); λ is the wavelength (m), T is the thermodynamic temperature of the blackbody (K); c_1 is the first radiation constant ($c_1 = 3.7419\times10^{-16}\ \mathrm{W}\cdot\mathrm{m}^2$); and c_2 is the second radiation constant ($c_2 = 1.4388\times10^{-2}\ \mathrm{m}\cdot\ \mathrm{K}$).

We denote the stellar spectral emissivity as $\varepsilon_{\lambda_1-\lambda_2}$. The band radiation power is

$$E_{\lambda_1-\lambda_2}=\varepsilon_{\lambda_1-\lambda_2}\cdot E_{\mathrm{b}(\lambda_1-\lambda_2)}, \quad (2)$$

and the band radiation intensity is

$$I_{\lambda_1-\lambda_2}=E_{\lambda_1-\lambda_2}/\pi. \quad (3)$$

The radius of the effective stellar temperature for the calculation is r, and the distance between the stellar surface and the receiving surface of the detector is R. Then, the solid angle between the stellar surface and the detector is

$$d\Omega = dA_{\mathrm{s}}/R^2 = \pi r^2/R^2. \quad (4)$$

A schematic diagram of the solid angle is shown in Figure 1. The band radiation power received at the detector is

$$E_{\mathrm{p}(\lambda_1-\lambda_2)} = d\Omega\cdot I_{\lambda_1-\lambda_2}. \quad (5)$$

The band radiation power received at the detector can be calculated from Equations (1) - (5), and is defined as

$$E_{\mathrm{p}(\lambda_1-\lambda_2)} = \frac{r^2}{R^2}\cdot\varepsilon_{\lambda_1-\lambda_2}\cdot\int_{\lambda_1}^{\lambda_2}\frac{c_1\lambda^{-5}}{\exp[c_2/(\lambda T)]-1}d\lambda. \quad (6)$$

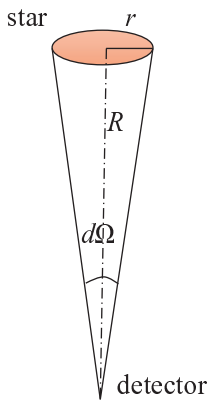

Fig. 1 Schematic diagram of the stellar solid angle.

Thus, we can define the stellar detected angular parameter as

$$\xi_{\lambda_1-\lambda_2} = \varepsilon_{\lambda_1-\lambda_2} \cdot \left(r^2/R^2\right). \tag{7}$$

Equation (6) can be written as

$$E_{\mathrm{p}(\lambda_1-\lambda_2)} = \xi_{\lambda_1-\lambda_2} \cdot \int_{\lambda_1}^{\lambda_2} \frac{c_1\lambda^{-5}}{\exp[c_2/(\lambda T)]-1} d\lambda, \tag{8}$$

which can be used to determine the band radiation power received at the detector that is above the Earth. In other words, the band radiation power received at the detector is calculated using the stellar effective temperature (T_{eff}) and the detected angular parameter ($\xi_{\lambda_1-\lambda_2}$), which is,

$$E_{\mathrm{p}(\lambda_1-\lambda_2)} = f\left(T_{\mathrm{eff}}, \xi_{\lambda_1-\lambda_2}\right). \tag{9}$$

Because the stellar surface contains gases that have different temperatures, pressures and densities, some bands have significant absorption or emission lines. Therefore, the radiation power from the stellar band is not exactly the same as a blackbody. To be more specific, there are differences from an ideal blackbody in some bands. This deviation is defined as the gray rate, ($\delta_{\lambda_1-\lambda_2}$). Equation (9) can also be written as

$$E_{\mathrm{p}(\lambda_1-\lambda_2)} = f\left(T_{\mathrm{eff}}, \xi_{\lambda_1-\lambda_2}, \delta_{\lambda_1-\lambda_2}\right). \tag{10}$$

2.2 Acquisition of Parameters in the Stellar Effective Temperature Model

The average radiation flux data for a fixed band can be obtained using a satellite detector, but the radiation flux data of other bands cannot. To solve this problem, we consider the following. We calculate effective stellar temperatures and detected angular parameters using inversion and several fixed band average radiation flux data. We can use this model to get stellar flux data in any band.

Therefore, we regard the physical model established in Section 2.1 as the direct problem, and use stochastic particle swarm optimization (SPSO) to solve the inverse problem. This process is illustrated in Figure 2.

The direct problem can be described as follows. First, we calculate the radiation power of some bands using known stellar effective temperatures and detected angular parameters. Then, we determine the average radiation flux density data. The corresponding inverse problem calculates some band radiation power using the average radiation flux density data. Then, stellar effective temperatures and detected angular parameters are calculated with an inverse method. The average flux density data are the driving source of the inverse problem. In this paper, these data were obtained from the Midcourse Space Experiment (MSX) catalog.

The MSX was launched by the United States in 1996, and has been used to study the Galactic plane and areas that are not covered by observations from the Infrared Astronomical Satellite (IRAS). MSX carries an infrared instrument called SPIRIT, which is a 35 cm aperture off-axis telescope with a high sensitivity. Data from version 2.3 of the MSX point source catalog were used in this paper. The MSX infrared photometric catalog contains data on 177 860 stars. Estimations of the right ascension, declination, proper motion and average flux density for six bands of stars are listed in the MSX catalog. The six bands are 6.8–10.8 μm, 4.22–4.36 μm, 4.24–4.45 μm, 11.1–13.2 μm, 13.5–15.9 μm and 18.2–25.1 μm. The flux density of radio sources is

$$S_v = (\theta, \phi)\cos\theta d\Omega, \tag{11}$$

where S_v ($\mathrm{W}\cdot\mathrm{m}^{-2}\cdot\mathrm{Hz}^{-1}$) represents the emitted energy.

The brightness of a radio source (also called its intensity) represents the emitted energy per unit frequency interval per unit area per unit time interval per unit solid angle. The integral illumination is obtained by multiplying the average energy density over the band. That is,

$$E_{\mathrm{p}(\lambda_1-\lambda_2)} = \int_{\lambda_1}^{\lambda_2} E_\lambda d\lambda = \int_{c/\lambda_1}^{c/\lambda_2} E_\gamma d\gamma, \tag{12}$$

which corresponds to the radiation power in the frequency interval. The MSX catalog table contains estimations of the average flux density for six bands of stars. We can determine the radiation power of these six bands.

We cannot determine analytical solutions because the equation is nonlinear. We apply numerical methods to the inverse problem. Additionally, it is difficult to define general numerical methods that produce satisfactory results because the range of effective stellar temperatures is large and detected angular parameters may range over several orders of magnitude. We apply the particle swarm optimization (PSO) algorithm that was proposed by Eberhart et al. (1995) and Kennedy (2007). The algorithm can find a global optimal solution or a good approximate solution. It can escape from a local minimum in solution space in order to find a global optimal solution. PSO has been studied extensively and applied to many fields. Recently, the SPSO algorithm has been developed. Yuan et al. (2010) used SPSO to calculate the inverse problem for atmospheric aerosol size distribution. Qi et al. (2008, 2011)

Table 2 Radiation Power in Six Bands at Different Effective Temperatures

Initial parameters		Band radiation power (10^{-16} W · m^{-2})					
Detected angular parameters	Effective temp. (K)	6.8–10.8 (μm)	4.22–4.36 (μm)	4.24–4.45 (μm)	11.1–13.2 (μm)	13.5–15.9 (μm)	18.2–25.1 (μm)
2×10^{-19}	1000	15.039	2.611	3.841	2.661	1.601	1.234
	5000	172.210	75.497	108.222	22.736	12.359	82.945
	10000	377.966	181.093	258.973	48.369	26.005	17.184

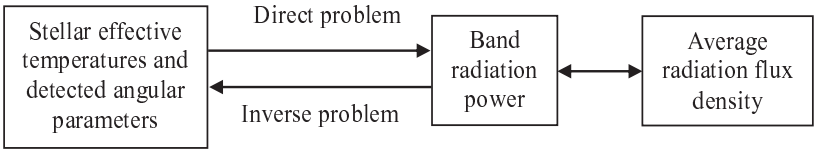

Fig. 2 Direct and inverse problems of derived stellar parameters.

adopted PSO to analyze the inverse transient radiation in one-dimensional non-homogeneous participating slabs and retrieve properties of participating media using different spans of radiation signals. Wang et al. (2011) calculated the absorption coefficient in a one-dimensional medium and reconstructed the coal fire depth profile using SPSO. We applied the SPSO algorithm to solve the inverse problem of effective stellar temperatures and detected angular parameters.

2.3 Analysis of the PSO and the SPSO Algorithms

In standard PSO, every possible solution is represented as a particle in a population, and each particle has its own position and velocity related to the inverse problem. All particles in the solution space search for the global optimum by pursuing an optimal adaptation that is determined by an objective function.

The mathematical description of PSO is as follows. There are M particles in a D-dimensional search space, and the spatial position of each particle represents a potential solution. The position vector for particle i is $X_i = (x_{i1}, x_{i2}, \cdots, x_{iD})$, and the velocity vector is $V_i = (v_{i1}, v_{i2}, \cdots, v_{iD})$. The best position that this particle has experienced (i.e., individual best) is $P_i = (p_{i1}, p_{i2}, \cdots, p_{iD})$ and is denoted P_{best}. The corresponding best position of all the particles (i.e., global best) is denoted by $P_g = (p_{g1}, p_{g2}, \cdots, p_{gD})$. The particle velocity depends on the personal best and global best, and it is given by

$$\begin{aligned} V_i(t+1) =& wV_i(t) + c_1 r_1 [P_i(t) - X_i(t)] \\ &+ c_2 r_2 [P_g(t) - X_i(t)]. \end{aligned} \tag{13}$$

Here, t is the current iteration, w is the inertia weight, c_1 and c_2 are constant accelerations, and r_1 and r_2 are random numbers in $[0, 1]$. The new location of X_i is

$$X_i(t+1) = X_i(t) + V_i(t+1). \tag{14}$$

Table 3 Different Combination Plans

Different Plans	Band Combinations (μm)
Plan A	6.8–10.8, 4.22–4.36, 4.24–4.45
Plan B	6.8–10.8, 4.24–4.45, 13.5–15.9
Plan C	6.8–10.8, 4.24–4.45, 18.2–25.1
Plan D	6.8–10.8, 13.5–15.9, 18.2–25.1
Plan E	4.22–4.36, 4.24–4.45, 11.1–13.2
Plan F	11.1–13.2, 13.5–15.9, 18.2–25.1

We set $w = 0$, and then get

$$\begin{aligned} X_i(t+1) =& X_i(t) + c_1 r_1 [P_i(t) - X_i(t)] \\ &+ c_2 r_2 [P_g(t) - X_i(t)]. \end{aligned} \tag{15}$$

This formula reduces the global search capability, but increases the local search capability. So, if $X_j(t) = P_j = P_g$, particle j will "fly" at a velocity of zero. To improve the global search capability, we conserve the current best position of the swarm P_g and particle j's best position P_j, then give a new position $X_j(t+1)$ to particle j, and other particles are manipulated according to Equation (15), thus the global search capability is enhanced. Because of the need to sample the particle's position from the domain when $X_j(t) = P_j = P_g$, the modified PSO algorithm is called SPSO.

The standard PSO algorithm may prematurely converge to suboptimal solutions that are not even guaranteed to be local extrema. By contrast, the SPSO, which is developed based on the analysis of standard PSO, is more efficient because of its local search capability according to Cui et al. (2004). The SPSO algorithm was compared with the PSO algorithm in the following, and then the optimal choice was obtained.

We used the following computational procedure to solve the stellar parameters problem.

Step 1: Set the input parameters of the system. The population size is set to 50, but it is adjustable and changeable. The maximum number of iterations is 3000. There are two variables and we set the acceleration constants to $c_1 = 1.80$ and $c_2 = 1.80$. We assume that the effective tempera-

ture is within $1000-20\,000$ K and that the detected angular parameters are between 1.0×10^{-21} and 1.0×10^{-16}. In this algorithm, we expand the above parameters to meet the computing requirements. That is, the range of effective temperatures is set to $1.0\times10^{2.5}-1.0\times10^{4.5}$ K, and the range of detected angular parameters is set to $1.0\times10^{-26}-1.0\times10^{-10}$. This determines the boundary of the solution space.

Step 2: Calculate the fitness value of each particle. A particle's fitness value is equal to its objective function value. The objective function is

$$\text{Fitnes } s_i=\sqrt{\left[\left(E_{ipa}-E_{ipb}\right)/E_{ipa}\right]^2}, \qquad (16)$$

where E_{ipa} represents the initial value of the inversion and E_{ipb} represents the value for particle i.

Step 3: Compare the fitness value of each particle with the a priori best, P_i. If the fitness is lower than P_i, set this value as the current P_i, and record the corresponding particle position.

Step 4: Compare the fitness value of each particle with the a priori best P_g; if the fitness is lower than P_g, set this value as the current P_g, and record the corresponding particle position.

Step 5: Generate the new particle, and update the velocity and position of other particles using Equations (13) and (15). If $X_j(t)=P_j=P_g$, the position of particle j is generated randomly.

Step 6: Check the stopping criteria. If the pre-set maximum number of generations is reached or if no improvement to the best solution is obtained after a given number of iterations, then the process is terminated. Otherwise, we increment the iteration index $(t=t+1)$ and go back to Step 2.

We compared the performances of the PSO and SPSO algorithms. For standard PSO, $w=1.0$, and for SPSO $w=0.0$. There were two termination criteria: (1) when the iteration accuracy was below a fixed level of 10^{-10} and (2) when we reached more than 3000 generations. We used five particles for both algorithms. The results are compared in Figure 3. The SPSO algorithm converged much faster than the standard PSO algorithm. Moreover, the SPSO algorithm found better values than the standard PSO algorithm with a smaller number of generations. Therefore, we applied SPSO to solve the stellar parameters problem.

3 NUMERICAL EXPERIMENTS AND RESULTS

Stellar effective temperatures and detected angular parameters can be calculated using the above SPSO algorithm if the stellar band radiation power is known. The accuracy of results is related to initial values of parameters in the inversion algorithm, the selected inversion bands and the applicable inversion temperature range. To verify the accuracy and stability of the SPSO algorithm for calculating stellar effective temperatures and detected angular parameters, we analyzed the following examples and studied the three factors separately.

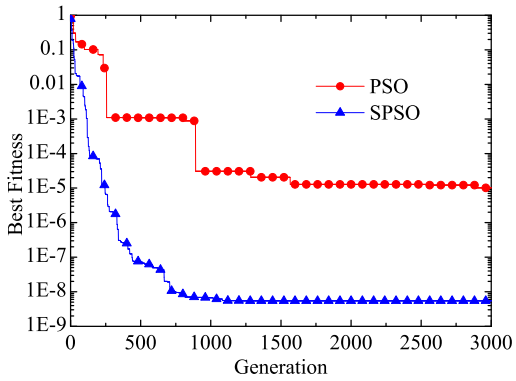

Fig. 3 Comparison of the values found by PSO and SPSO.

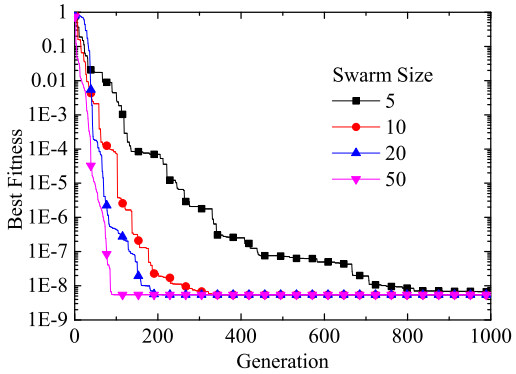

Fig. 4 Comparison of the best fitness values for different swarm sizes.

The six band radiation power is different if effective temperatures and detected angular parameters are different. Table 2 shows the band radiation power data for different initial temperatures.

Case 1. Number of particles

The number of particles in the SPSO algorithm has an important effect on the inversion efficiency, and it is directly related to the accuracy. Thus, we must determine the optimal number of particles.

We set the number of particles to 5, 10, 20 and 50 and calculated the results in Figure 4. An increase of the particle number corresponds to a decrease in the number of generations required for the algorithm to converge. When the convergence value was set to 1.0×10^{-8}, 749 generations were required when there were five particles, whereas only 86 generations were required when there were 50 particles.

When calculating effective temperatures and detected angular parameters, nonlinearities mean that more particles significantly increase the computation time, but do not help the convergence of the residual. Therefore, considering the computation time and the accuracy, we selected 50 particles.

Case 2. Selection of the inversion band

From the six bands of the MSX catalog, three bands of radiation power data were used as initial values for the inversion. The six combinations (Plans A, B, C, D, E and F) are shown in Table 3.

Table 4 Relative Errors for Different Gray Deviations When $T_{\rm eff} = 1000$ K using SPSO

Parameter	True value	$\gamma = 0$		$\gamma = 5$		$\gamma = 15$		$\gamma = 30$	
		SPSO	$\varepsilon_{\rm rel}\%$	SPSO	$\varepsilon_{\rm rel}\%$	SPSO	$\varepsilon_{\rm rel}\%$	SPSO	$\varepsilon_{\rm rel}\%$
$T_{\rm eff}$	1000.0	1000.0	0.000	999.3	0.069	1001.4	0.142	1014.8	1.4805
$\zeta \times 10^{-19}$	2.0000	2.0000	0.000	2.0163	0.813	2.0211	1.057	1.9534	2.329

Table 5 Relative Errors for Different Gray Deviations When $T_{\rm eff} = 10\,000$ K using SPSO

Parameter	True value	$\gamma = 0$		$\gamma = 5$		$\gamma = 15$		$\gamma = 30$	
		SPSO	$\varepsilon_{\rm rel}\%$	SPSO	$\varepsilon_{\rm rel}\%$	SPSO	$\varepsilon_{\rm rel}\%$	SPSO	$\varepsilon_{\rm rel}\%$
$T_{\rm eff}$	10000.0	10000.0	0.000	9724.2	2.758	9633.0	3.670	10876.9	8.769
$\zeta \times 10^{-19}$	2.0000	2.0000	0.000	2.0763	3.813	2.1138	5.688	1.8436	7.820

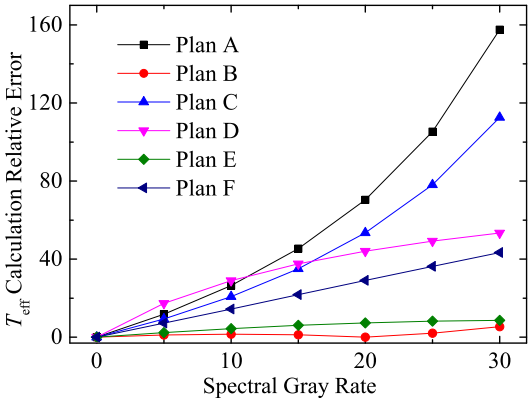

Fig. 5 $T_{\rm eff}$ relative error compared with the gray rate for the six plans.

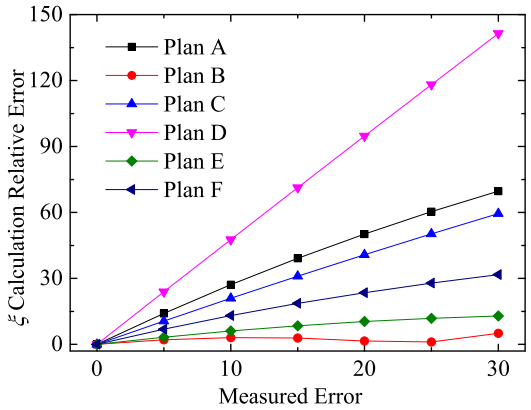

Fig. 6 Relative error compared with the gray rate for the six plans.

Stellar effective temperatures and detected angular parameters depend on the inversion plans. This reflects the different properties of the estimated parameters.

To demonstrate the effect of the gray rate (δ) on the inverse parameters, we added random standard deviations to the exact parameters computed from the direct problem. That is,

$$Y_{\rm mea} = Y_{\rm exact} + \sigma \cdot \varsigma, \tag{17}$$

where ς is a normally distributed random variable with zero mean and unit standard deviation. The standard deviation of the measured $E_{\lambda_1-\lambda_2}$, for a measured error γ at 99% confidence is

$$\sigma = (Y_{\rm exact} \times \gamma\%)\,/2.576. \tag{18}$$

For comparison, the relative error is

$$\varepsilon_{\rm rel} = 100 \times (Y_{\rm est} - Y_{\rm exact})\,/Y_{\rm exact}. \tag{19}$$

The stellar effective temperature was set to 5000 K, and the detected angular parameter was set to 2.0×10^{-19}. We then calculated radiation flux data for the six bands. Normally distributed deviations were added to the radiation flux data, and then the data with no deviations were used to solve the inverse calculations of the effective temperature and detected angular parameter. The data for the six plans are shown in Table 3. The variations of the effective temperature and detected angular parameter with gray deviations are shown in Figures 5 and 6 respectively.

As shown in Figures 5 and 6, the relative errors of the six plans were very close to 0 when there were no gray deviations. The estimated parameters are very consistent with the true values. This shows that each plan satisfies the requirement that there are no gray deviations. When there were gray deviations, an increase in gray deviations corresponded to an increase in the relative error of the effective temperature and detected angular parameter. The relative errors for Plans A, C and D increased more rapidly and significantly than the gray rate. When the gray rate increased by 30%, the effective temperature for Plans A and C increased by 157.5% and 112.7% respectively, while the detected angular parameter of Plan D increased by 141.4%. This shows that there are strong absorption or emission lines when using these three plans, and that they produce the effective temperature and detected angular parameter values that represent deviations from the initial spectral radiation power data.

The inversion results for Plans B, E, and F were relatively good, as shown by the detailed errors in Figures 7 and 8. The inversion results for Plan B were the closest to the true values. When the gray rate increased by 30%, the relative errors in the effective temperature and detected angular parameter increased by 5.4% and 5.1% respectively. Therefore, the relative errors of the inversion results were much smaller than the gray deviations, indicating that the inversion results for Plan B were the best.

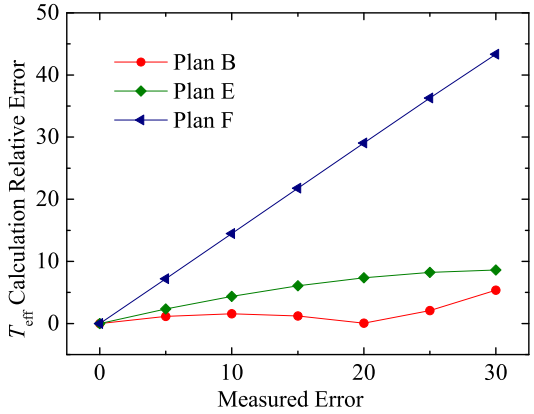

Fig. 7 $T_{\rm eff}$ relative error compared with the gray rate for the three plans.

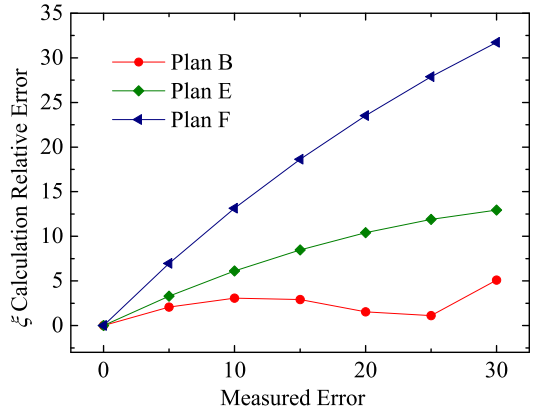

Fig. 8 Relative error compared with the gray rate for the three plans.

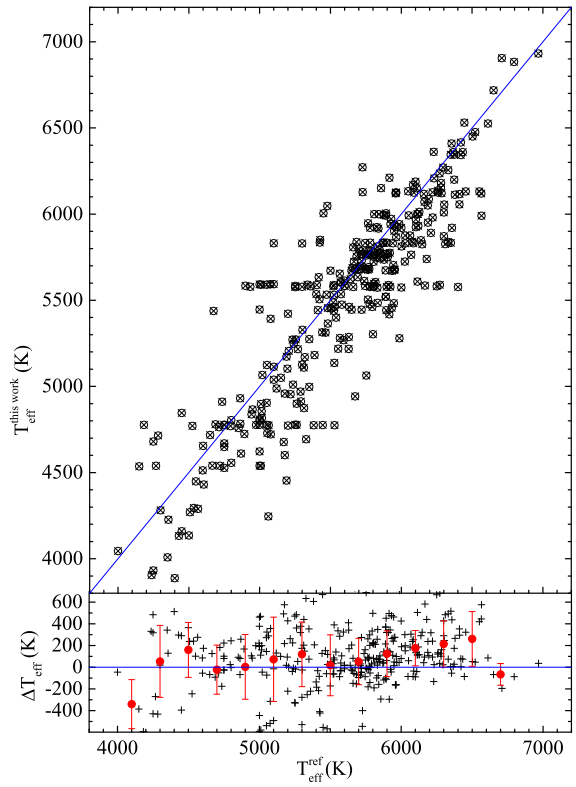

Fig. 9 Comparison of effective temperatures in the literature and estimated values in this work. The differences $\Delta T_{\rm eff} = \left(T_{\rm eff}^{\rm ref} - T_{\rm eff}^{\rm thiswork}\right)$ are plotted at the bottom (with red dots and error bars representing the means and standard deviations of differences respectively in the individual temperature bins).

In the above results, the effective temperature was set to 5000 K. Considering the large range of effective temperature, different effective temperatures correspond to different bands of radiation power. We must verify the accuracy of the results for different effective temperatures.

Next, we verified the accuracies of stellar effective temperatures and detected angular parameters for different radiation power data obtained from different effective temperatures (1000 K and 10 000 K).

We then set the effective temperature to 1000 K or 10 000 K, and used the obtained band radiation power in the inverse problem. The results are shown in Tables 4 and 5. When the effective temperature was 1000 K and the gray rate increased by 30%, the relative errors in the effective temperature and detected angular parameter only increased by 1.4805% and 2.329% respectively. When the effective temperature was 10 000 K, the relative errors in the effective temperature and detected angular parameter only increased by 8.769% and 7.820% respectively. The relative errors in the inversion parameters were much smaller than the gray rate, and the estimates were close to the initial data. Therefore, the inversion requirement was satisfied.

The relative errors in the estimates obtained by the inverse calculations are less than the gray deviations of the raw data for different effective temperatures. Plan B can be used to calculate the raw data without gray deviations, and to calculate the original data with gray deviations.

Case 3. The impact of repeated calculations on the inversion results

Repeated calculations affect the inversion results. As shown in Table 6, when the effective temperature was 5000 K, the detected angular parameter was 2.0×10^{-19} and the gray deviation was 30%, the relative errors changed with repeated calculations. The relative error of the effective temperature was stable at 5.369% and the relative error of the detected angular parameter was stable at 5.098%. This shows that the method can stably calculate the effective temperature and the detected angular parameter.

Our analysis below is based on the above results. Although the maximum radiation flux was for Plan A, the radiation wavelength interval was too small. This resulted in a large inversion error. There were long bands of 18.2–25.1 μm for Plans C and D, which also caused large inversion errors. However, Plan B did not have these problems, and produced the best inversion results. It used larger band intervals of 6.8–10.8 μm, 4.24–4.45 μm and 13.5–15.9 μm, which have big radiation fluxes. So, we used Plan B

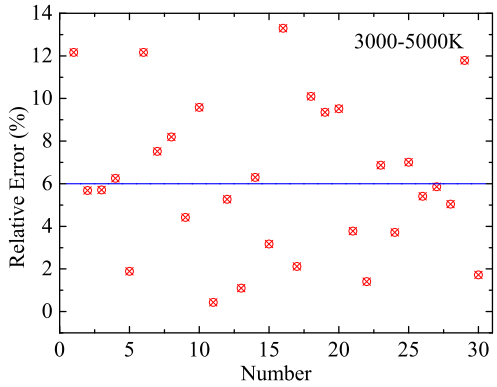

Fig. 10 Relative errors for different $T_{\rm eff}$ between 3000–5000 K.

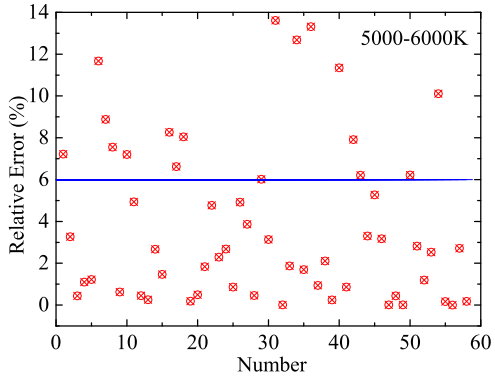

Fig. 11 Relative errors for different $T_{\rm eff}$ between 5000–6000 K.

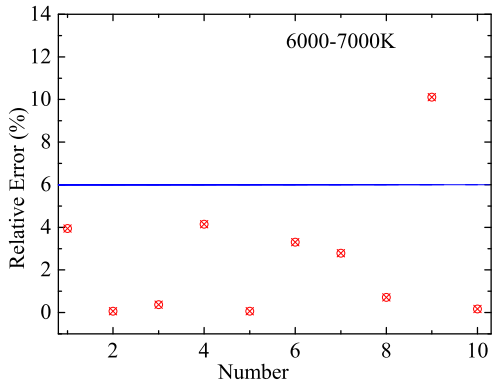

Fig. 12 Relative errors for different $T_{\rm eff}$ between 6000–7000 K.

as the inverse solution for the stellar flux data of the MSX catalog.

4 DATA COMPARISON AND ANALYSIS

The results of the above numerical experiments demonstrated that the model and SPSO algorithm produced highly accurate and stable calculations of stellar effective temperatures and detected angular parameters. We determined the accuracy using an error analysis with different temperatures and different band combinations, and checked the stability by analyzing repeated calculations. This model and algorithm can solve the stellar flux data inversion problem for effective temperatures between 1000 and 20 000 K, with detected angular parameters between $1.0\times10^{-21}-1.0\times10^{-16}$ and a gray rate below 30%. When calculating the radiation flux data for the MSX catalog, we used the parameter settings and algorithm suggested by the above analysis.

Table 6 Results for Different Numbers of Calculations, Demonstrating the Stability of the Inversion.

Calculation numbers	Effective temperatures (K)	Error (%)	Detected angular parameters (10^{-19})	Relative error (%)
1	5268.4705	5.369	1.8980343	5.098
2	5268.4714	5.369	1.8980339	5.098
3	5268.4711	5.369	1.8980340	5.098
4	5268.4711	5.369	1.8980340	5.098
5	5268.4706	5.369	1.8980343	5.098
6	5268.4713	5.369	1.8980339	5.098
7	5268.4694	5.369	1.8980348	5.098
8	5268.4693	5.369	1.8980348	5.098
9	5268.4702	5.369	1.8980344	5.098
10	5268.4705	5.369	1.8980343	5.098

We calculated the stellar effective temperatures and detected angular parameters for the MSX catalog using the average radiation flux data for each band based on the proposed algorithm.

Figure 9 compares our results with 336 true values known in literatures (Alves-Brito et al. 2010; Bergemann & Gehren 2008; Bihain et al. 2004; Burris et al. 2000; Carney et al. 2003; Charbonnel & Primas 2005; Fulbright & Johnson 2003; Gratton et al. 2000; Hansen et al. 2012; Ishigaki et al. 2010; Gratton et al. 2003; Ishigaki et al. 2012; Jonsell et al. 2005; Ishigaki et al. 2013; Mishenina & Kovtyukh 2001; Reddy et al. 2006; Roederer et al. 2008; Saito et al. 2009; Simmerer et al. 2004; Takada-Hidai et al. 2002; Takeda & Honda 2005; Van Eck et al. 2003; Yong et al. 2003; Fulbright 2000; Høg et al. 2000; Monet et al. 2003; Marshall 2007; Kiraga 2012). The estimated effective temperatures are consistent with previously reported data. The errors are shown at the bottom in Figure 9. Most errors were less than 10%, except for those corresponding to individual stars. These inversion results are quite reliable.

Stellar effective temperatures calculated using the MSX catalog are mostly concentrated in 3000–7000 K. The relative errors are different within this temperature range. The relative errors for three temperature ranges (3000–5000 K, 5000–6000 K and 6000–7000 K) are shown in Figures 10, 11 and 12 respectively. We can use these results to determine the best inversion temperature range for this computational model. The errors were uniformly distributed around 6% for effective temperatures of 3000–5000 K, whereas they were mostly less than 6% for effective temperatures of 5000–6000 K. The overwhelming majority of errors were less than 6% for effective temperatures of 6000–7000 K. Therefore, this model is most suitable for high temperatures between 6000–7000 K. This conclusion is consistent with the theory. According to

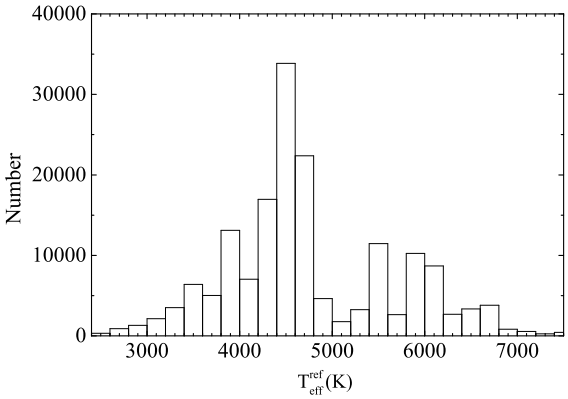

Fig. 13 Histogram distribution of stellar effective temperatures in the MSX catalog.

Plank's law, higher effective temperatures correspond to larger radiation fluxes. The impact of high temperature is smaller than that of low temperature at the same gray rate.

The histogram distribution of $T_{\rm eff}$ in the MSX catalog is plotted as Figure 13. As we can see, the stellar effective temperatures mainly range from 3000 K to 7000 K, and temperature from 4000 K to 6000 K is a hot region. The errors in these ranges are acceptable. The means of differences in individual temperature bins from 4300 K to 6000 K are close to 0 K, and the errors of temperatures are within 200 K. The model and method can be applied to calculation of temperatures using the MSX catalog.

5 SUMMARY

We used features of stellar spectral radiation and sky surveys to establish a computational model for stellar effective temperatures, detected angular parameters and gray rates. We applied known stellar flux data in some bands to determine stellar effective temperatures and detected angular parameters using SPSO. We first verified the reliability of the SPSO algorithm, and then found reasonable parameters that produced accurate estimates under certain gray deviation levels. Finally, we calculated 177 860 stellar effective temperatures and detected angular parameters using the MSX catalog data. We found that the estimated stellar effective temperatures were very accurate when compared with stellar effective temperatures that are published in literatures. We selected bands of 6.8–10.8 μm, 4.24–4.45 μm and 13.5–15.9 μm in our inversion. Our results were very accurate. The gray deviation has a smaller impact on the inversion results if the bands are closer to shorter wavelengths for temperatures of 6000–7000 K. This work makes full use of catalog data and presents a new way of studying stellar characteristics. It proposes a novel way of calculating stellar effective temperatures and detected angular parameters.

Acknowledgements This work was supported by the National Natural Science Foundation of China (Grant Nos. 51327803 and 51406041), and the Fundamental Research Funds for the Central Universities (Grant No. HIT. NSRIF. 2014090). A very special acknowledgement is made to the editors and referees who made important comments that improved this paper.

References

Ahn, C. P., Alexandroff, R., Allende Prieto, C., et al. 2012, ApJS, 203, 21
Aihara, H., Allende Prieto, C., An, D., et al. 2011, ApJS, 193, 29
Alves-Brito, A., Meléndez, J., Asplund, M., Ramírez, I., & Yong, D. 2010, A&A, 513, A35
Bailer-Jones, C. A. L. 2000, A&A, 357, 197
Bergemann, M., & Gehren, T. 2008, A&A, 492, 823
Bihain, G., Israelian, G., Rebolo, R., Bonifacio, P., & Molaro, P. 2004, A&A, 423, 777
Blackwell, D. E., Petford, A. D., & Shallis, M. J. 1980, A&A, 82, 249
Blackwell, D. E., & Shallis, M. J. 1977, MNRAS, 180, 177
Burris, D. L., Pilachowski, C. A., Armandroff, T. E., et al. 2000, ApJ, 544, 302
Carney, B. W., Latham, D. W., Stefanik, R. P., Laird, J. B., & Morse, J. A. 2003, AJ, 125, 293
Charbonnel, C., & Primas, F. 2005, A&A, 442, 961
Cohen, M. 1993, AJ, 105, 1860
Cui, Z. H., Zeng, J. C., & Cai, X. 2004, in Evolutionary Computation, 2004. CEC2004. Congress on, 1, IEEE, 316
Eberhart, R. C., Kennedy, J., et al. 1995, in Proceedings of the Sixth International Symposium on Micro Machine and Human Science, 1, New York, NY, 39
Egan, M. P., Price, S. D., & Kraemer, K. E. 2003, The Midcourse Space Experiment Point Source Catalog Version, 2, 2114
Engelke, C. W., Price, S. D., & Kraemer, K. E. 2006, AJ, 132, 1445
Fulbright, J. P. 2000, AJ, 120, 1841
Fulbright, J. P., & Johnson, J. A. 2003, ApJ, 595, 1154
Gratton, R. G., Carretta, E., Claudi, R., Lucatello, S., & Barbieri, M. 2003, A&A, 404, 187
Gratton, R. G., Sneden, C., Carretta, E., & Bragaglia, A. 2000, A&A, 354, 169
Hansen, C. J., Primas, F., Hartman, H., et al. 2012, A&A, 545, A31
Høg, E., Fabricius, C., Makarov, V. V., et al. 2000, A&A, 355, L27
Huang, Y., Liu, X.-W., Yuan, H.-B., et al. 2015, MNRAS, 454, 2863
Ishigaki, M., Chiba, M., & Aoki, W. 2010, PASJ, 62, 143
Ishigaki, M. N., Chiba, M., & Aoki, W. 2012, ApJ, 753, 64
Ishigaki, M. N., Aoki, W., & Chiba, M. 2013, ApJ, 771, 67
Ishihara, D., Onaka, T., Kataza, H., et al. 2010, A&A, 514, A1
Jonsell, K., Edvardsson, B., Gustafsson, B., et al. 2005, A&A, 440, 321
Katz, D., Soubiran, C., Cayrel, R., Adda, M., & Cautain, R. 1998, A&A, 338, 151

Kennedy, J. 2007, Genetic Programming and Evolvable Machines, 8, 107
Kiraga, M. 2012, Acta Astronomica, 62, 67
Kordopatis, G., Gilmore, G., Steinmetz, M., et al. 2013, AJ, 146, 134
Luo, A.-L., Zhao, Y.-H., Zhao, G., et al. 2015, RAA (Research in Astronomy and Astrophysics), 15, 1095
Marshall, J. L. 2007, AJ, 134, 778
Mishenina, T. V., & Kovtyukh, V. V. 2001, A&A, 370, 951
Monet, D. G., Levine, S. E., Canzian, B., et al. 2003, AJ, 125, 984
Neugebauer, G., Habing, H. J., van Duinen, R., et al. 1984, ApJ, 278, L1
Qi, H., Ruan, L. M., Shi, M., An, W., & Tan, H. P. 2008, J. Quant. Spec. Radiat. Transf., 109, 476
Qi, H., Wang, D. L., Wang, S. G., & Ruan, L. M. 2011, J. Quant. Spec. Radiat. Transf., 112, 2507
Rebassa-Mansergas, A., Agurto-Gangas, C., Schreiber, M. R., Gänsicke, B. T., & Koester, D. 2013, MNRAS, 433, 3398
Rebassa-Mansergas, A., Gänsicke, B. T., Schreiber, M. R., Koester, D., & Rodríguez-Gil, P. 2010, MNRAS, 402, 620
Rebassa-Mansergas, A., Nebot Gómez-Morán, A., Schreiber, M. R., et al. 2012, MNRAS, 419, 806
Reddy, B. E., Lambert, D. L., & Allende Prieto, C. 2006, MNRAS, 367, 1329
Ren, J. J., Rebassa-Mansergas, A., Luo, A. L., et al. 2014, A&A, 570, A107
Roederer, I. U., Lawler, J. E., Sneden, C., et al. 2008, ApJ, 675, 723
Saito, Y.-J., Takada-Hidai, M., Honda, S., & Takeda, Y. 2009, PASJ, 61, 549
Simmerer, J., Sneden, C., Cowan, J. J., et al. 2004, ApJ, 617, 1091
Skrutskie, M. F., Cutri, R. M., Stiening, R., et al. 2006, AJ, 131, 1163
Soubiran, C., Katz, D., & Cayrel, R. 1998, A&AS, 133, 221
Steinmetz, M., Zwitter, T., Siebert, A., et al. 2006, AJ, 132, 1645
Takada-Hidai, M., Takeda, Y., Sato, S., et al. 2002, ApJ, 573, 614
Takeda, Y., & Honda, S. 2005, PASJ, 57, 65
Van Eck, S., Goriely, S., Jorissen, A., & Plez, B. 2003, A&A, 404, 291
Wang, Y., Wang, D., Shi, G., & Zhong, X. 2011, Sensor Letters, 9, 1952
Wright, E. L., Eisenhardt, P. R. M., Mainzer, A. K., et al. 2010, AJ, 140, 1868
Xiang, M. S., Liu, X. W., Yuan, H. B., et al. 2015, MNRAS, 448, 822
Yong, D., Lambert, D. L., & Ivans, I. I. 2003, ApJ, 599, 1357
Yuan, H.-B., Liu, X.-W., Huo, Z.-Y., et al. 2015, MNRAS, 448, 855
Yuan, Y., Yi, H.-L., Shuai, Y., Wang, F.-Q., & Tan, H.-P. 2010, J. Quant. Spec. Radiat. Transf., 111, 2106
Zhang, J. N., Wu, F. C., Luo, A. L., & Zhao, Y. H. 2005, Spectroscopy and Spectral Analysis, 25, 2088
Zhao, G., Zhao, Y.-H., Chu, Y.-Q., Jing, Y.-P., & Deng, L.-C. 2012, RAA (Research in Astronomy and Astrophysics), 12, 723